

VESPA

Vaso per Esperimenti Su Plasmi ed Altro

Andrea Grossutti, mat. 1237344
Alessandro Lovo, mat. 1236048
Leonardo Zampieri, mat. 1237351

December 26, 2019

1 Aims

Study the *Vespa* experimental apparatus, and in particular:

- Model the vacuum system behavior, finding the characteristic parameters;
- Obtain the current-voltage and the current-temperature characteristics curves of the filament;
- Draw the voltage-current characteristics curves of the gas discharge, enhancing their behavior as varying pressure;
- Find the Paschen curve, both in DC and RF condition;
- Measurement of plasma parameters through a Langmuir probe, both in stationary conditions and via ionic-sonic wave propagation.

2 Vacuum system

The vacuum inside the VESPA vessel (a cylindrical vessel, with a length of $\sim 80\text{cm}$ and a radius of $\sim 20\text{cm}$: $V \sim 0.1\text{m}^3$) is obtained and kept thanks to a rotary pump and a turbomolecular pump. The vessel is not perfectly isolated and some small leaks affect the vacuum keeping. To study this phenomena, the vessel has been taken to a low pressure ($\sim 6 \cdot 10^{-5}\text{mbar}$) and all the valves around have been closed. Isolating the chamber from the pumping system one can measure (thanks to a ionization pressure gauge) the pressure in the vessel as function of time. Effects as leaks and degasing contribute to an inflow in the chamber $F_0(p)$ that in principle could depend on the pressure. Assuming instead F_0 constant, its value can be estimated through a linear fit on the data: $P = a + b \cdot t$, $F_0 = V \cdot b$.

Considering the reaction time, the slowness of the ionization gauge in stabilizing and the pressure oscillations, the errors are estimated as 5% on the pressure and 0.5s error on the time.

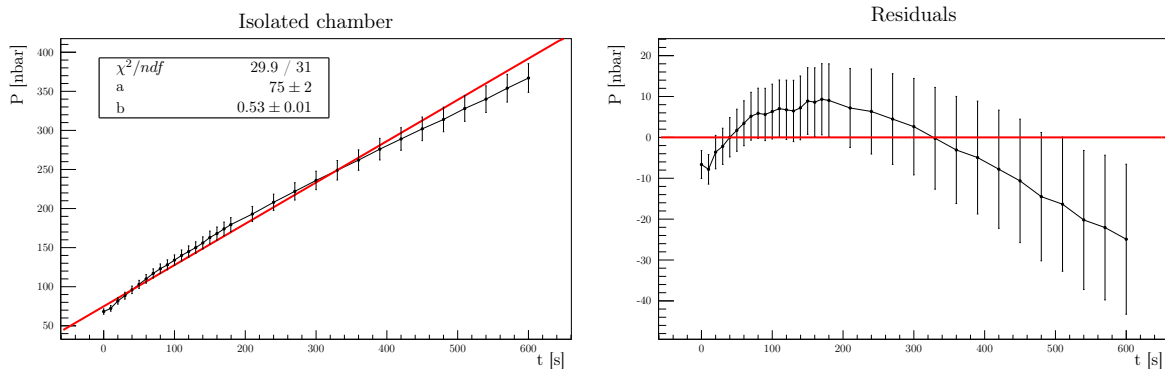


Figure 1: Presure increasing in the chamber

As can be seen from fig 1 there is an evident trend in the residuals, proving that F_0 cannot be assumed constant throughout all the explored range of pressures. A possible way to correct this is to

consider a low pressure regime and a high pressure one: the limit has been put where the trend in the residuals inverts, i.e. around 200nPa.

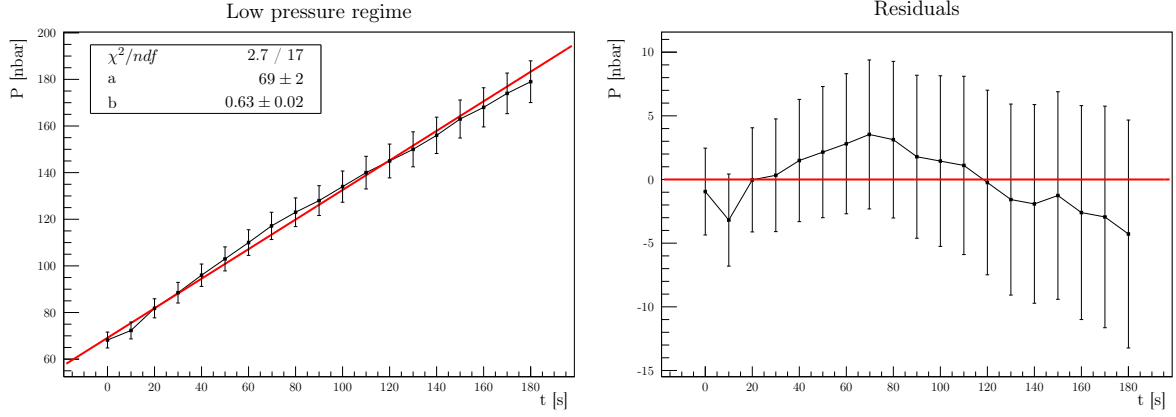


Figure 2: Low pressure regime

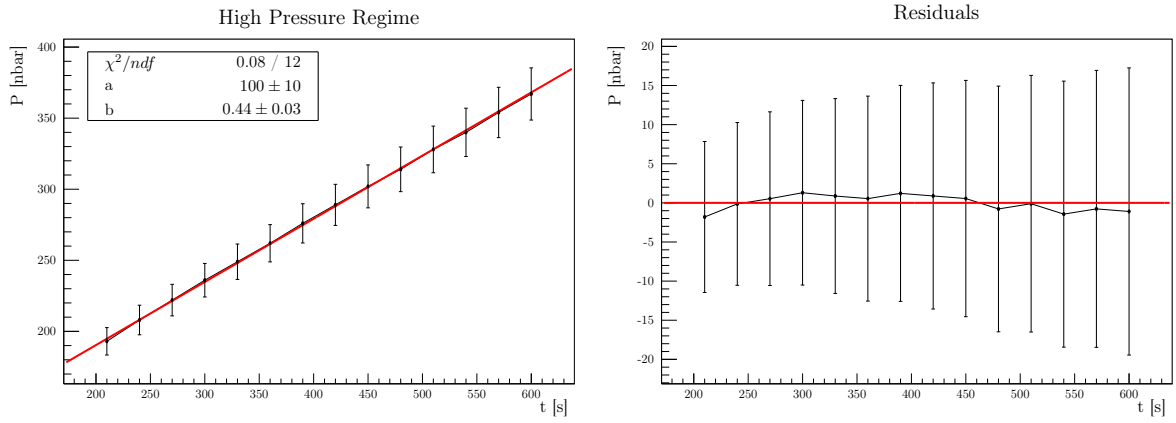


Figure 3: High pressure regime

Splitting the high pressure regime and the low pressure one two different estimation of the inflow can be computed:

$$F_0^{\text{low}} = (6.4 \pm 0.4) \cdot 10^{-6} \text{Pa m}^3/\text{s}, \quad F_0^{\text{high}} = (4.5 \pm 0.4) \cdot 10^{-6} \text{Pa m}^3/\text{s}$$

where a 5% error on the volume is assumed.

Subsequently, the valve has been opened connecting the chamber to the pumping system. An exponential lowering of the pressure is expected: $P(t) = (P_i - P_0)e^{-t/\tau} + P_0$, where P_i is the starting pressure and P_0 the asymptotic one.

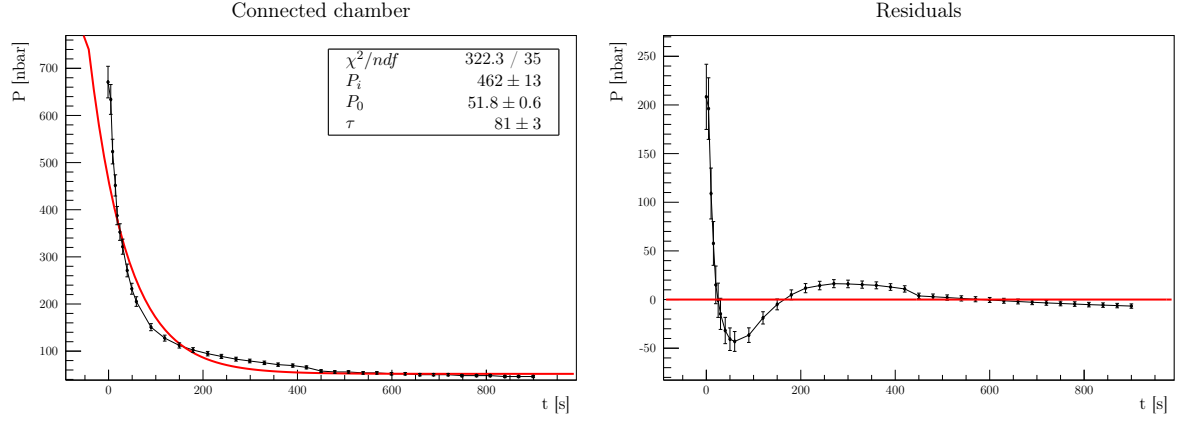


Figure 4: Pressure lowering in the chamber

As can be seen from fig 4, similarly as what seen before, the result are not acceptable and as before two regimes can be distinguished. For coherence and for a better comparison, the same limit previously chosen has been used.

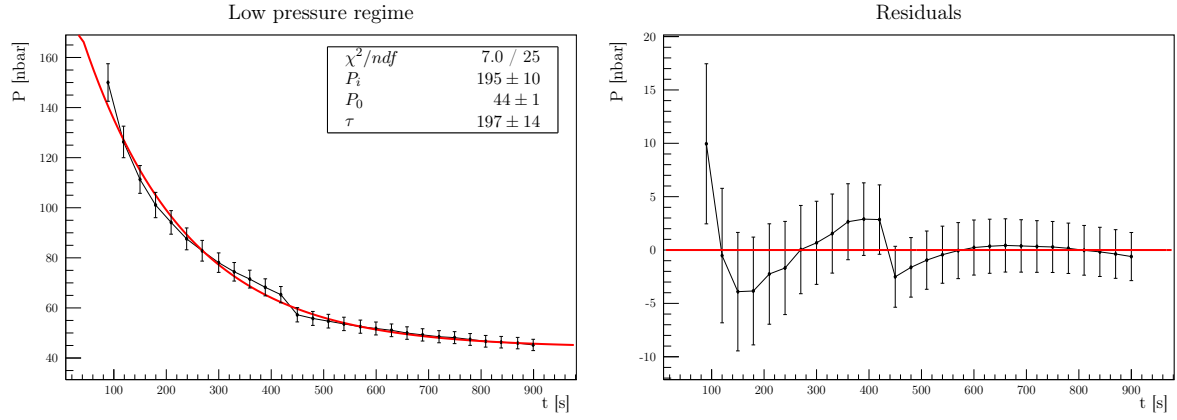


Figure 5: Low pressure regime

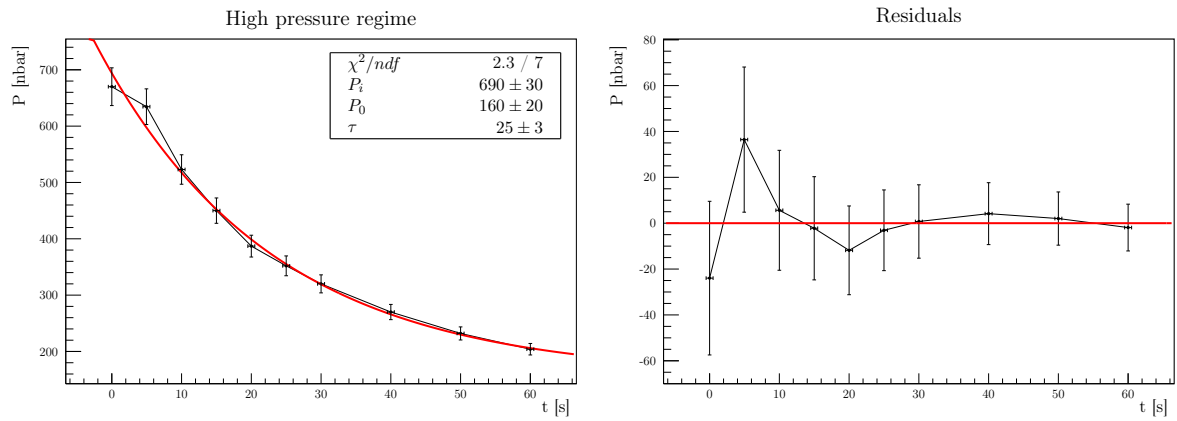


Figure 6: High pressure regime

Performing two separate exponential fits, they result in a meaningful result (even if a small trend in residual is still visible). From the values of τ and P_0 the effective pumping speed S_e , the inflow F_0 and, given the nominal value of the pumping speed $S = 331/\text{s}$, the conductance of the chamber-pump connection C can be estimated.

Regime	$S_e = v/\tau [\text{l s}^{-1}]$	$F_0 = P_0 \cdot S_e [\text{Pa m}^3/\text{s}]$	$C = (S_e^{-1} - S^{-1})^{-1} [\text{l s}^{-1}]$
Low pressure	0.51 ± 0.04	$(2.2 \pm 0.2) \cdot 10^{-6}$	0.52 ± 0.05
High pressure	4.0 ± 0.6	$(2 \pm 1) \cdot 10^{-5}$	4.6 ± 0.7

Table 1: Vacuum parameters

In the low pressure regime the two estimates of F_0 are not compatible but still comparable, while at high pressure the two estimates differ by an order of magnitude. Moreover, by comparing the nominal pumping speed with the effective one, a discrepancy can be observed; this can be due both to a low-conductance of the connection or a not-complete efficiency of the pump.

3 Voltage-Current characteristic of the filament

The filament inside the vessel is a tungsten filament with diameter $2r \sim 0.25\text{mm}$ and length $L \sim 10\text{cm}$. Combining Ohm law and emissivity rules, a theoretical characteristic curve can be obtained:

$$V = \frac{A^{10/7} L}{\pi^{13/7} r^{23/7} (2\epsilon\alpha)^{3/7}} \cdot I^{13/7}$$

where ϵ is the effective emissivity, α the Stefan Boltzmann constant and A the resistivity proportional constant, such that the resistivity ρ can be expressed as function of the temperature T as

$$\rho(T) = AT^{6/5}$$

Pumping the vessel to a low pressure ($\sim 3.7 \cdot 10^{-5}\text{mbar}$), the voltage-current characteristic curve of the filament has been measured, producing the following data:



Figure 7: Voltage-Current characteristic for a filament; errors has been chosen as $0.3A^{13/7}$ and $0.1V$, due to the low sensibility of the measure system.

Fitting the data with a $V \propto I^{13/7}$, the following parameters are found:

$$V = mI^{13/7} \tag{1}$$

$$m = (0.391 \pm 0.002)V \cdot A^{-13/7} \tag{2}$$

which lead to a value of

$$\epsilon \sim 0.2$$

The χ^2 confirm the meaningfulness of the fit; moreover, the effective emissivity has a value similar to the typical one (0.3).

Finally, the estimated filament temperature as a function of the driven current can be found:

$$T = \underbrace{\frac{A^{5/14}}{\pi^{5/7} r^{15/14} (2\epsilon\alpha)^{5/14}}}_k \cdot I^{5/7} \quad \text{with } k \sim 811 \text{K} \cdot \text{A}^{-5/7}$$

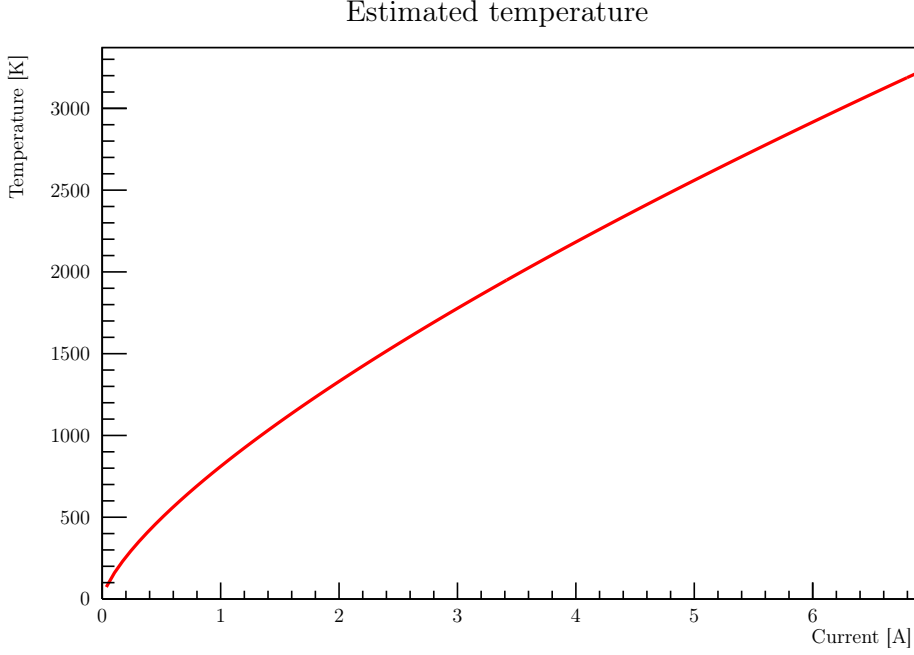


Figure 8: Projection of the filament temperature as function of the current

4 V-I characteristics of the discharge & DC Paschen curve

By polarizing the filament with respect to the whole vessel (grounded) a discharge in the plasma can be achieved. By measuring the polarization voltage on the power supply (0.1V estimated error) and the plasma current via the voltage across a resistor $R_{\text{shunt}} = (1.00 \pm 0.03)\Omega^*$, the discharge characteristic curve can be studied. In particular the breakdown is clearly visible.

*The errors on the voltage measurement is negligible with respect to the errors in the resistance, therefore only the latter has been considered.

4.1 Varying I_f

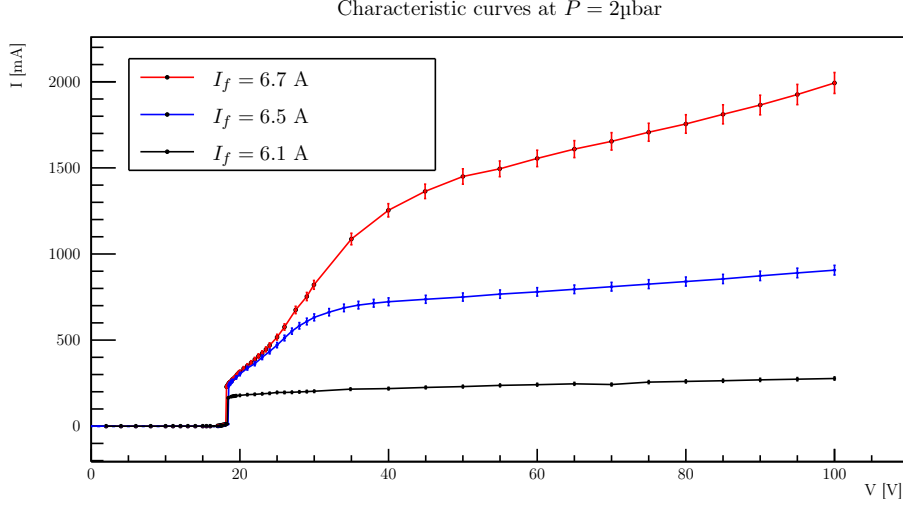


Figure 9: V-I characteristics of the discharge at constant pressure P , varying the filament current I_f . The breakdown is clearly visible around $\sim 18V$.

As can be seen from fig 9, variations on filament current doesn't affect breakdown voltage, but changes the behavior of the plasma once it is ignited.

The current emitted by the filament into the plasma can be modeled by Richardson law:

$$I = \Sigma A T^2 \exp\left(-\frac{e\Phi}{k_B T}\right)$$

where for our tungsten filament $A = 7 \cdot 10^5 \text{ A/m}^2 \text{K}^2$, $\Phi = 4.55 \text{ V}$ and $\Sigma = 2\pi r L \sim 80 \text{ mm}^2$ is the surface area of the filament. By using the previous found relation between the temperature and the filament current $T = k \cdot I_f^{5/7}$, and assuming that the plasma current is the whole current emitted by the filament, an expression for the current can be obtained:

$$I = J I_f^{10/7} \exp\left(-Q I_f^{-5/7}\right) \quad \text{where:} \quad J = \Sigma A k^2 \sim 3.6 \cdot 10^7 \text{ A}^{-3/7} \quad Q = \frac{e\Phi}{k_B k} \sim 65 \text{ A}^{5/7}$$

Richardson law predicts no dependence of the plasma current on the polarization voltage V , so a first comparison between the predicted plasma current and the experimental one is to use for the latter the value at $V = 60 \text{ V}$: value at which the plasma has been ignited but the electric field is not strong enough to induce a high multiplication of electrons.

$I_f [\text{A}, \pm 0.1]$	$I^{\text{exp}} [\text{A}, \pm 0.1]$	$I^{\text{Rich}} [\text{A}]$	$I^{\text{Rich}}/I^{\text{exp}}$
6.1	0.2	~ 8	~ 34
6.5	0.8	~ 20	~ 25
6.7	1.6	~ 30	~ 19

Table 2: Experimental plasma current at $V = 60 \text{ V}$ and prediction from Richardson law.

As can be seen from tab 2 the prediction are about ~ 25 times greater than the data. This can be due to an error in the estimate of coefficient k or in the assumption that the current emitted by the filament corresponds to the plasma current. The latter seems more reasonable, considering the behavior of electrons inside the plasma; in fact, they tend to form a cloud around the filament which prevent the emission of further electrons.

4.2 Varying P

By studying instead the V-I characteristics varying the Argon pressure one obtains the results in fig 10. It is visible that the pressure influence the breakdown voltage, effect that can be better understood building the experimental Paschen curve (fig 11): by setting the pressure in the chamber the breakdown voltage is found by slowly increasing the polarization potential until the plasma ignites.

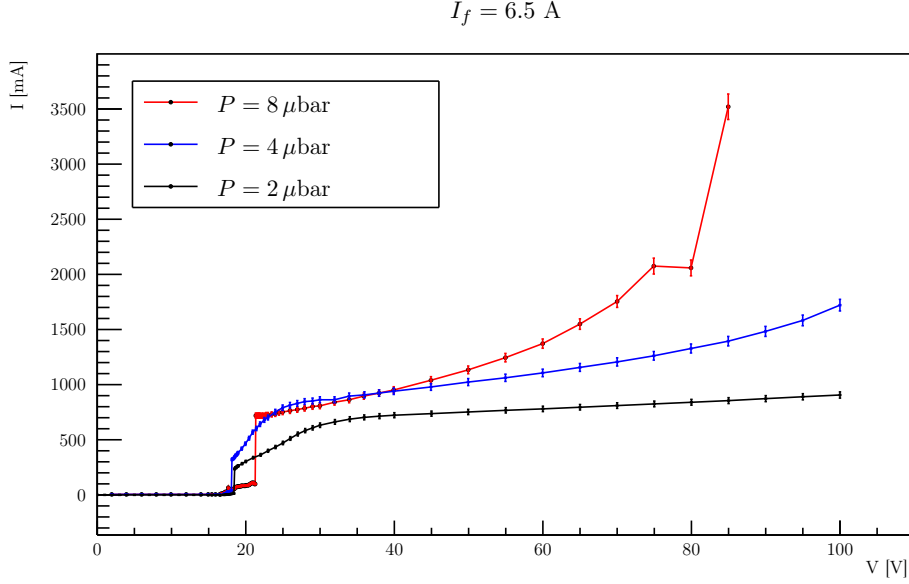


Figure 10: V-I characteristics of the discharge at constant filament current I_f , varying the pressure P . The last-but-one point in the red dataset is clearly false, so it has been neglected.

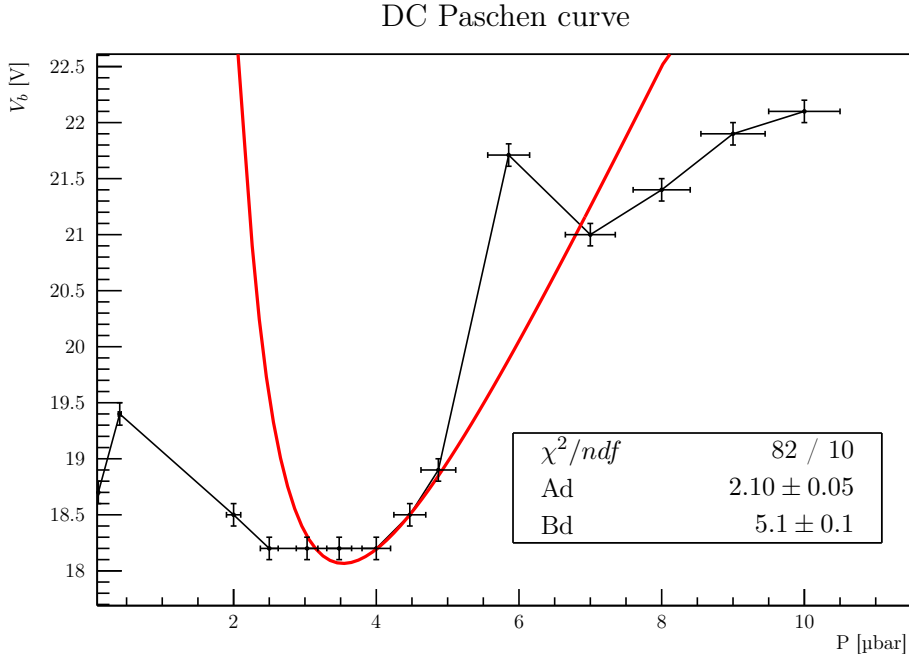


Figure 11: Paschen curve: breakdown voltage as function of the pressure; the theoretical Paschen curve (red) is clearly unable to fit the data.

The theoretical formula of the Paschen curve is

$$V_b = \frac{Bpd}{\log(Apd) - C} \quad (pd)_{min} = \frac{e^{1+C}}{A} \quad (3)$$

where d is the distance between the electrodes and for Argon $A = 8.63\text{m}^{-1}\text{Pa}^{-1}$, $B = 132.0\text{Vm}^{-1}\text{Pa}^{-1}$ and $C = 1.004$. By keeping C fixed[†] at the theoretical value and varying A and B it is possible to perform a fit on the data (fig 11). A way to compare the results of the fit with the theoretical ones is to take consider the ratio A/B :

$$\left(\frac{A}{B}\right)_{\text{experimental}} = \left(\frac{Ad}{Bd}\right) = (0.41 \pm 0.01)\text{V}^{-1} \quad \left(\frac{A}{B}\right)_{\text{theoretical}} \sim 0.07\text{V}^{-1}$$

As can be seen the experimental results do not agree with the theory both in the sense that the fit with the theoretical curve has a very high χ^2 and in the sense that the fitting parameters are incompatible with the expected theoretical values.

It can then be deduced that this system does not follow the theoretical Paschen's curve. A Paschen minimum can be however individuate as the range:

$$P_{\text{min,DC}} = 2.5\text{--}4 \cdot 10^{-3}\text{mbar}$$

5 Paschen curve in radiofrequency condition

Inside VESPA a magnetic antenna is provided, which allows to ignite the plasma through radiofrequency waves that, coupling with gas electrons, excite them and generate the discharge.

The antenna is powered through a RF generator and a RLC circuit; firstly, the response of the circuit is studied. Keeping fixed the generator power and varying the frequency, through an oscilloscope the peak-to-peak amplitude of the wave downstream the circuit is measured. The result is a typical resonance curve (fig. 12).

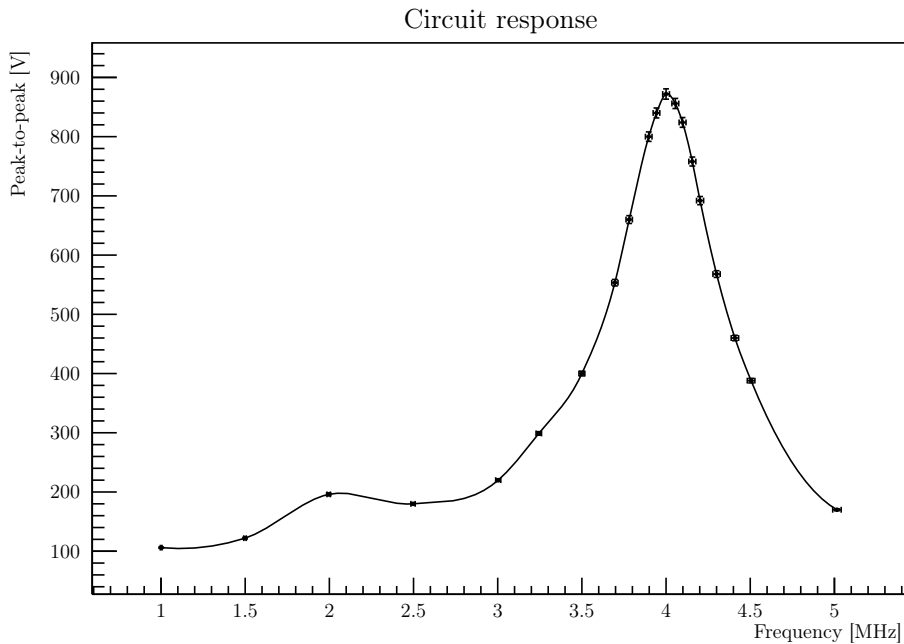


Figure 12: Peak-to-peak amplitude downstream the circuit, varying the wave frequency. From the oscillation in the measurements and the instrumentation sensibility, the errors has been estimated at 5‰ in the frequencies and 1% in voltages.

From the fig. 12 the maximum can be detected: it is around 4MHz. Therefore the operation area is identified in the range 3–4MHz, when the amplitude is high and increasing with the frequency.

Varying the pressure in the vessel, the breakdown voltage trend can be studied. For each pressure, the frequency has been increased until the discharge took place (it's a clearly visible phenomena, so

[†]Eventual variations of C can be absorbed into the variation of A , so keeping C fixed is not limiting.

the discrimination has been done visually), and the peak-to-peak voltage in the breakdown point has been measured. The result is the Paschen curve in fig. 13.

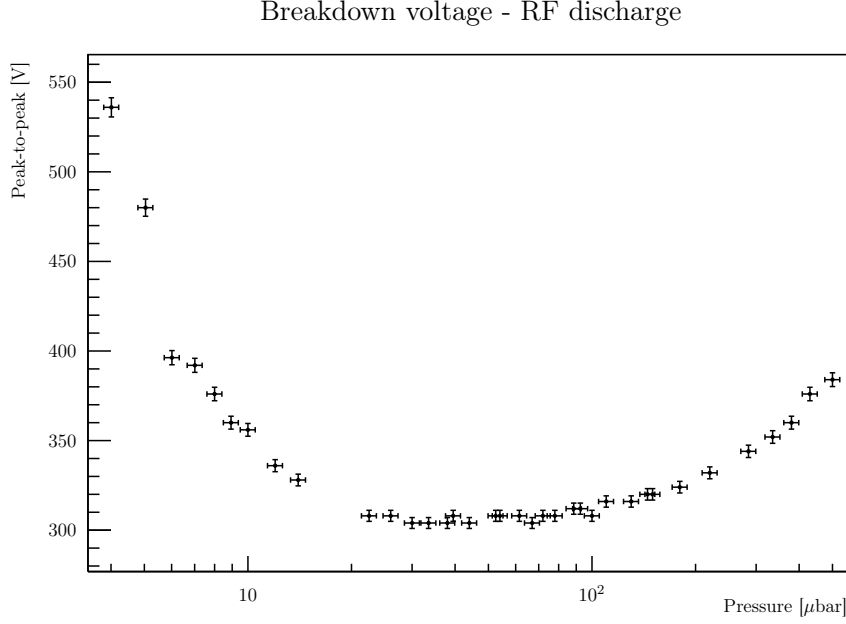


Figure 13: Radiofrequency Paschen curve. From the oscillation in the measurements and the instrumentation sensibility, the errors have been estimated at 5% in the pressures and 1% in voltages.

As can be seen from the plot, the minimum of the Paschen curve in radiofrequency condition is very wide: the optimal area can be identified in the range:

$$3-7 \cdot 10^{-5} \text{bar}$$

6 Measurement of plasma parameters

Using a Langmuir probe an estimate of plasma parameters, such as density, electron temperature and plasma potential, can be obtained. The electron current through the probe follows this relation:[‡]

$$I = I_{si} (1 + R(V - V_f)) \left(\exp \left(\frac{e(V - V_f)}{kT_e} \right) - 1 \right)$$

where I_{si} is the Ion Saturation Current, V_f the Floating Potential, T_e the Electronic Temperature and R an additional factor that describes the current-voltage characteristic for $V \ll V_f$. It is important to observe that the formula describes experimental data for $V \lesssim V_f$, while for higher values of V additional terms are required.

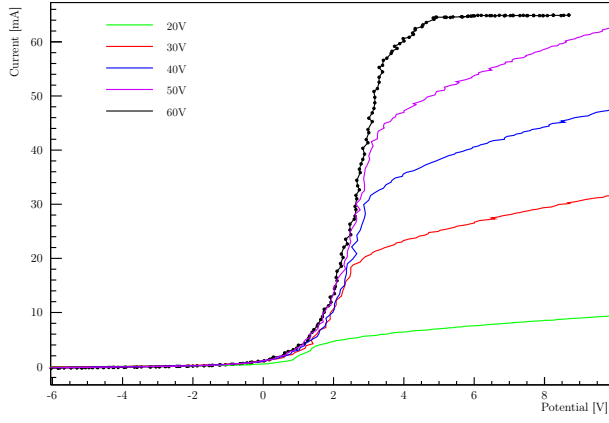
Other plasma parameters can be obtained with the following relations:

$$c_s = \left(\frac{eT_e}{m_i} \right)^{1/2} \quad n = \frac{2I_{si}}{e c_s A} \quad V_p = V_f + \frac{1}{2} \left(\log \left(\frac{m_i}{2\pi m_e} \right) + 1 \right) T_e$$

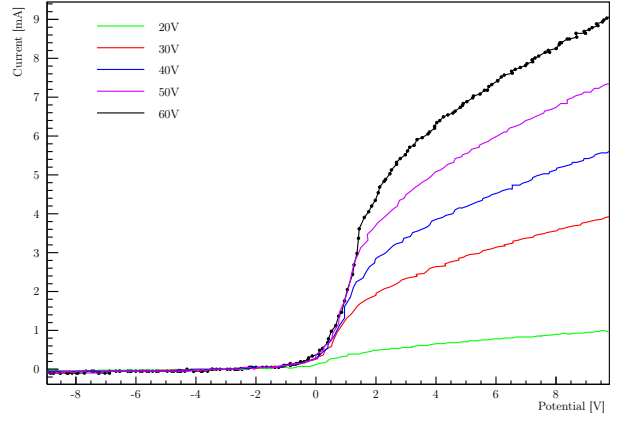
where c_s is the ionic-sonic speed, n the plasma density, V_p the plasma potential, m_i is the ion mass, A is the probe area and e is electron charge.

For the characterization of the plasma two Langmuir probes has been inserted in the chamber, one in the same side of the filament ("filament side"), and one in the opposite side, near the pumping group ("pump side").

[‡]This relation is a different version of the one derivated in D. Desideri and G.Serianni *Four Parameter data fit for Langmuir probes with nonsaturation of ion current*, Rev. Sci. Instrum., 69 (1998), <https://doi.org/10.1063/1.1148942>

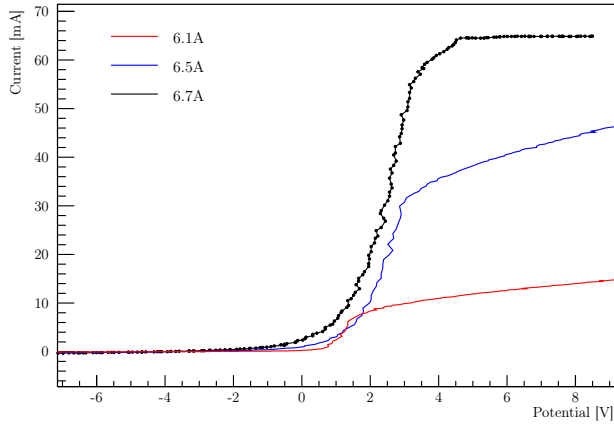


(a) Filament side

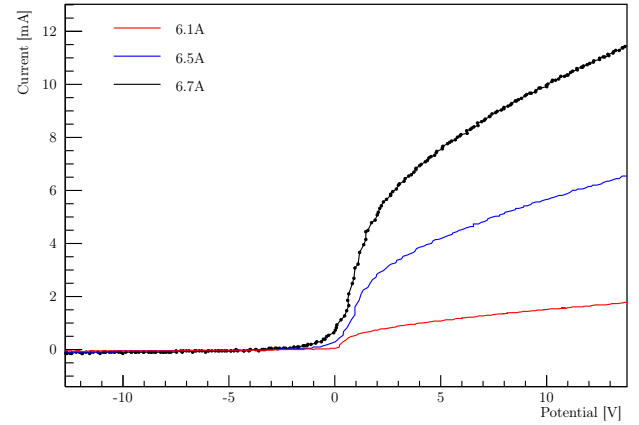


(b) Pump side

Figure 14: Electrical voltage–current characteristic of the Langmuir probe for a pressure of $2.84\mu\text{bar}$, a filament current of 6.5A and different discharge polarization voltages.

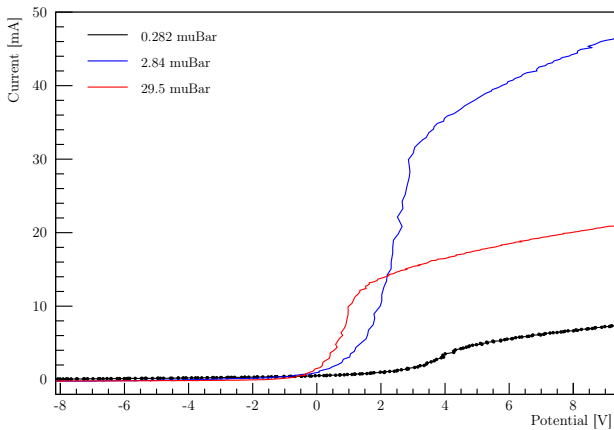


(a) Filament side

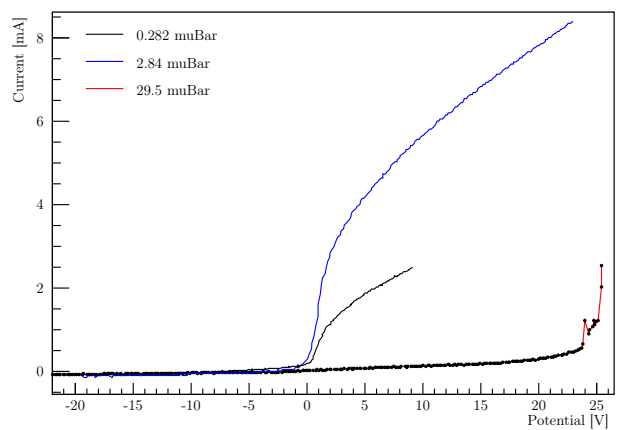


(b) Pump side

Figure 15: Electrical voltage–current characteristic of the Langmuir probe for a pressure of $2.84\mu\text{bar}$, a polarization voltage of 40V and different filament currents.



(a) Filament side



(b) Pump side

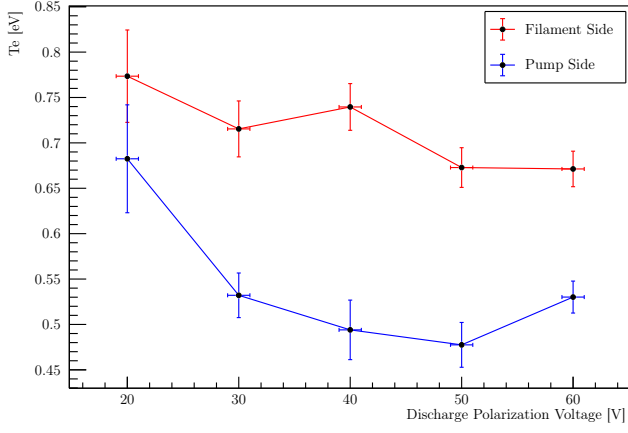
Figure 16: Electrical voltage–current characteristic of the Langmuir probe for a filament current of 6.5A , a polarization voltage of 40V and different pressure.

Plasma parameters are obtained from the characteristics through interpolations and the previous relations, and are represented with respect to several apparatus parameters.

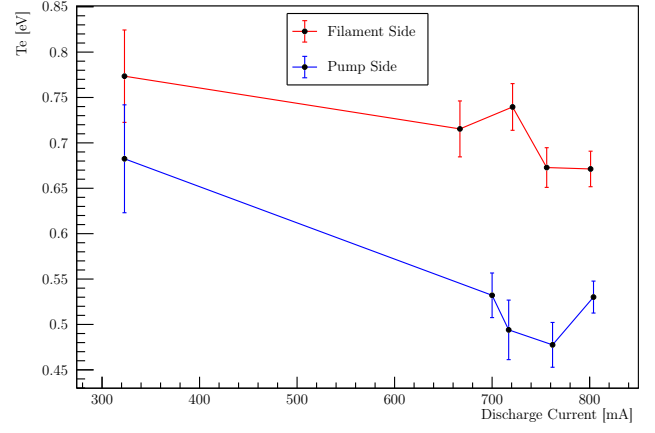
Error bars take into account uncertainty in data acquisition and fitting parameters estimation errors. Systematic errors have not been taken into account. Notice that small variations in the range

where V–I characteristic has been considered raise to quite different results in the analysis.

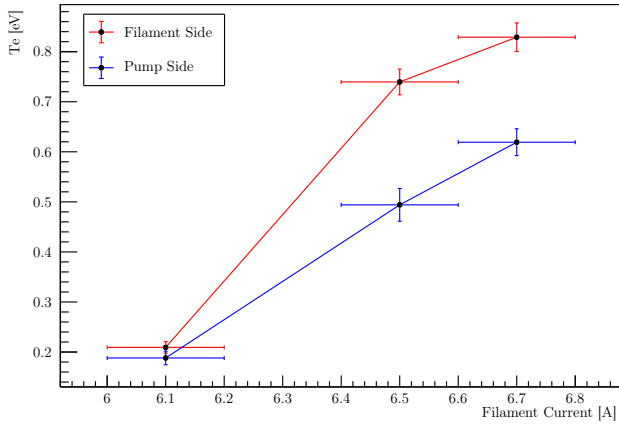
6.1 Electronic temperature



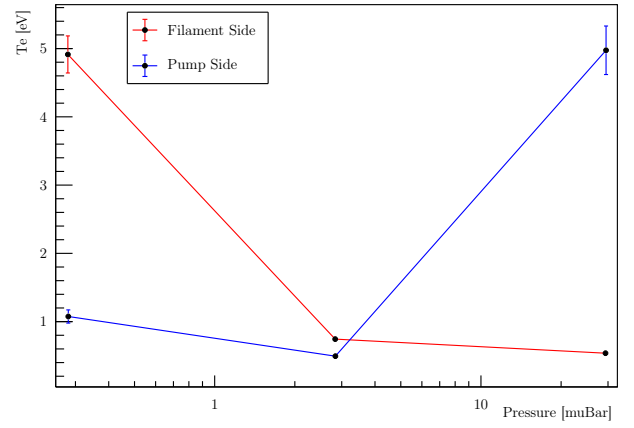
(a) Dependence on discharge polarization voltage, for a pressure of $2.84\mu\text{bar}$ and a filament current of 6.5A



(b) Dependence on discharge current, for a pressure of $2.84\mu\text{bar}$ and a filament current of 6.5A .



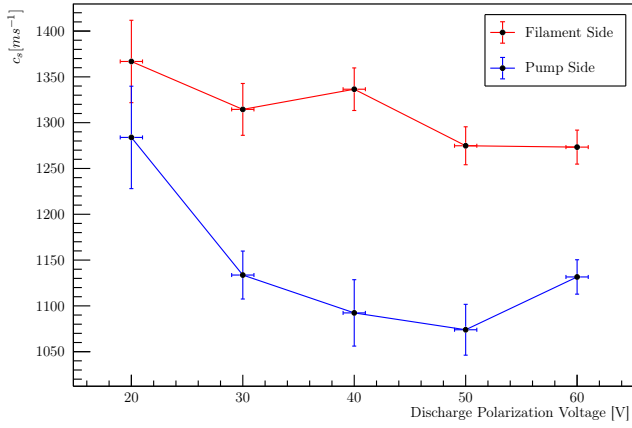
(c) Dependence on filament current, for a pressure of $2.84\mu\text{bar}$ and a polarization voltage of 40V .



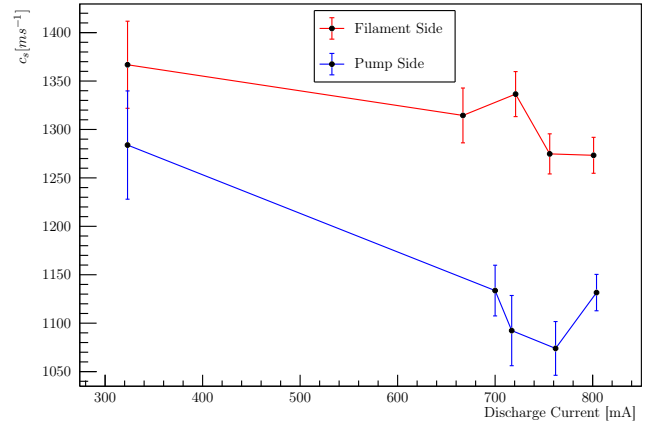
(d) Dependence on the chamber pressure, for a filament current of 6.5A and a polarization voltage of 40V .

Figure 17: Dependence of electronic temperature on different parameters.

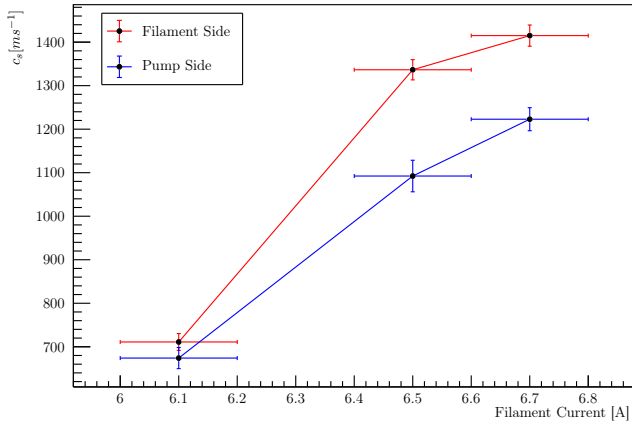
6.2 Ionic-sonic speed



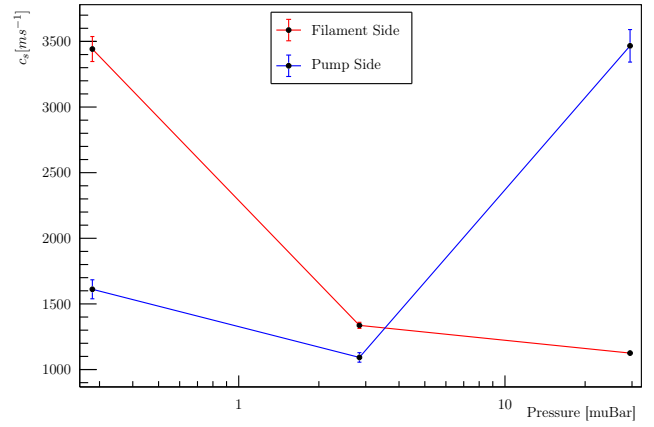
(a) Dependence on discharge polarization voltage, for a pressure of $2.84\mu\text{bar}$ and a filament current of 6.5A



(b) Dependence on discharge current, for a pressure of $2.84\mu\text{bar}$ and a filament current of 6.5A .



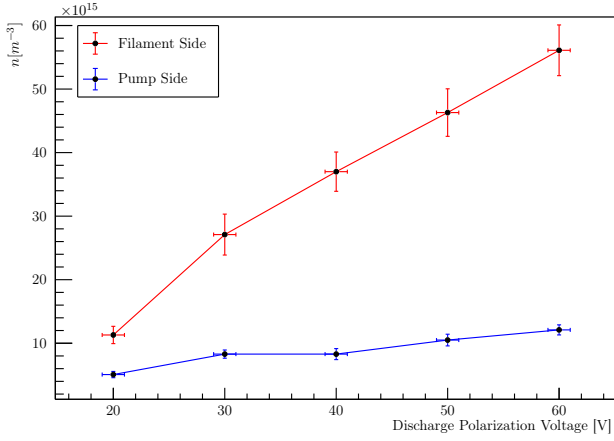
(c) Dependence on filament current, for a pressure of $2.84\mu\text{bar}$ and a polarization voltage of 40V .



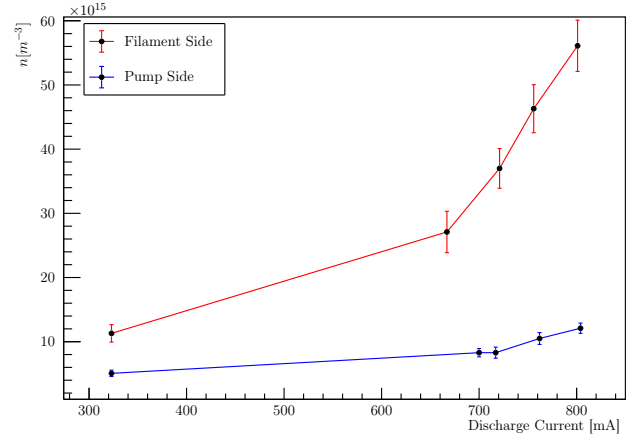
(d) Dependence on the chamber pressure, for a filament current of 6.5A and a polarization voltage of 40V .

Figure 18: Dependence of ion average velocity on different parameters.

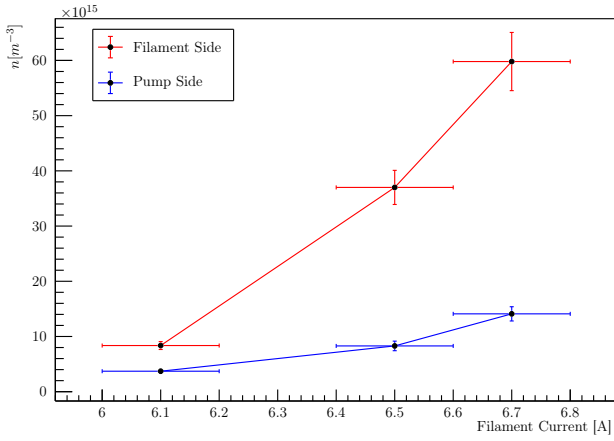
6.3 Plasma density



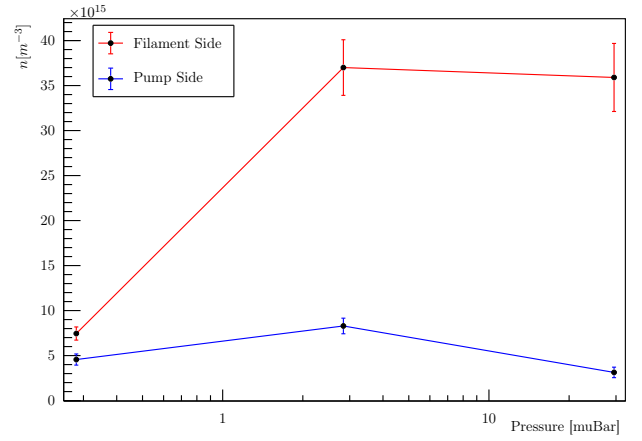
(a) Dependence on discharge polarization voltage, for a pressure of $2.84\mu\text{bar}$ and a filament current of 6.5A



(b) Dependence on discharge current, for a pressure of $2.84\mu\text{bar}$ and a filament current of 6.5A .



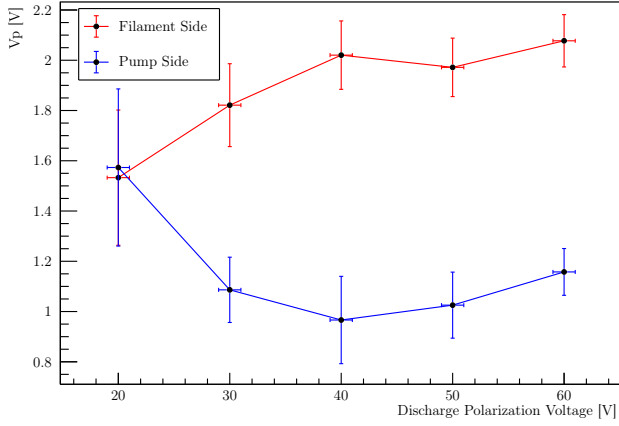
(c) Dependence on filament current, for a pressure of $2.84\mu\text{bar}$ and a polarization voltage of 40V .



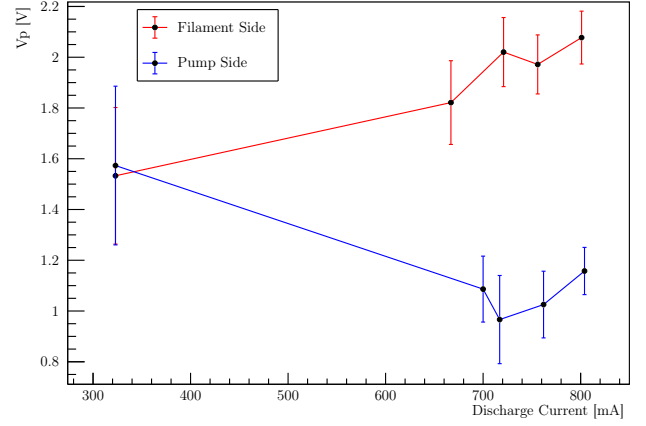
(d) Dependence on the chamber pressure, for a filament current of 6.5A and a polarization voltage of 40V .

Figure 19: Dependence of plasma density on different parameters.

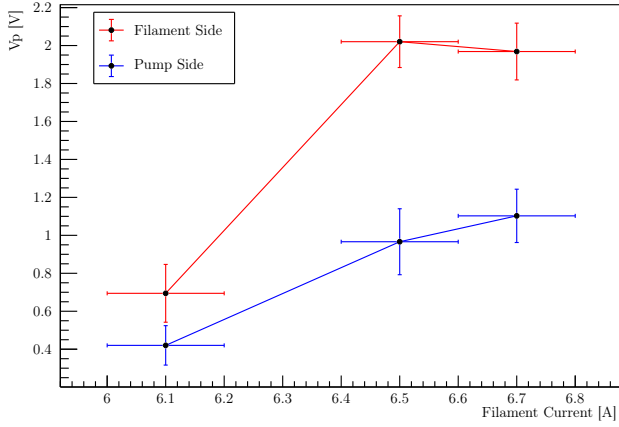
6.4 Plasma potential



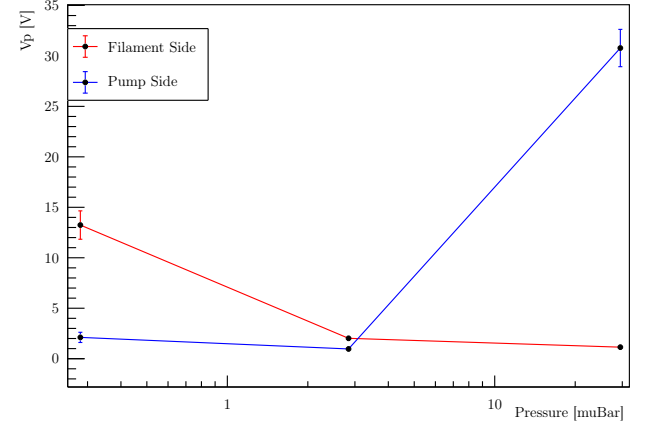
(a) Dependence on discharge polarization voltage, for a pressure of $2.84\mu\text{bar}$ and a filament current of 6.5A



(b) Dependence on discharge current, for a pressure of $2.84\mu\text{bar}$ and a filament current of 6.5A .



(c) Dependence on filament current, for a pressure of $2.84\mu\text{bar}$ and a polarization voltage of 40V .



(d) Dependence on the chamber pressure, for a filament current of 6.5A and a polarization voltage of 40V .

Figure 20: Dependence of plasma potential on different parameters.

6.5 Ionization fraction

The ionization fraction f of the plasma can be derived from previous parameters with the relation:

$$f = \frac{n}{n + n_0}$$

where n is the plasma density, and n_0 is the neutral atom gas density at room temperature ($T = (19 \pm 3)^\circ\text{C}$) obtained through ideal gas law since the gas is neutral:

$$n = \frac{P}{kT}$$

The error estimation must be considered as an upper bound to the uncertainty, since from the definition follows that $f < 1$.

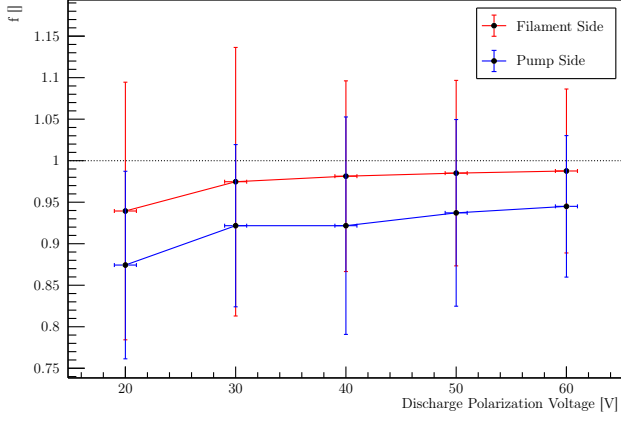
From these graphs we can conclude that for a pressure in the order of magnitude of μbar the ionization fraction near the filament is in the range

$$92 - 98\%$$

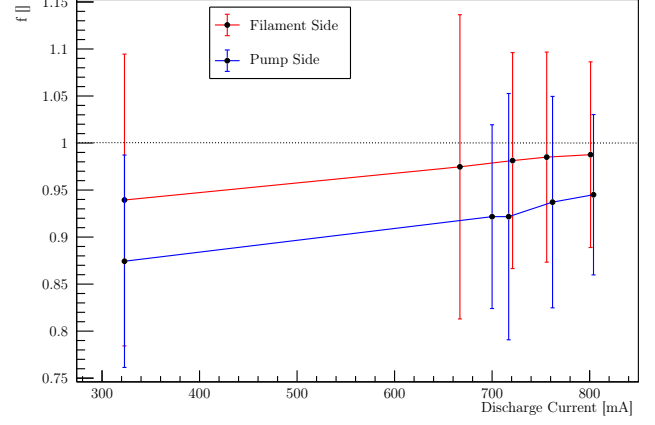
while near the pumping system smaller fraction are obtained due to the distance from the electrons emitter filament:

$$85 - 94\%$$

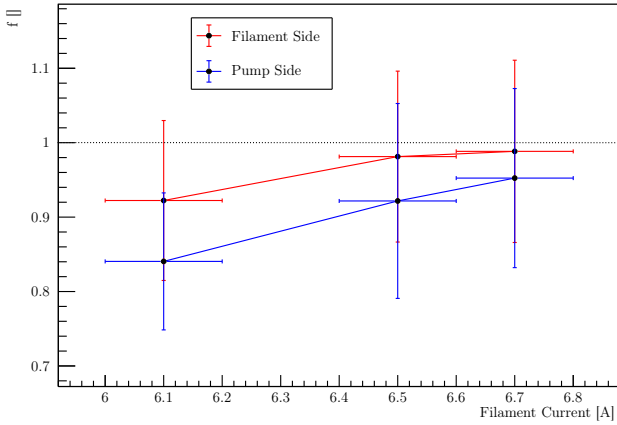
The graph 21(d) shows that the ionization fraction decreases fastly when pressure increase. This can be related to the smaller free path of electrons due to higher number of atoms in the chamber.



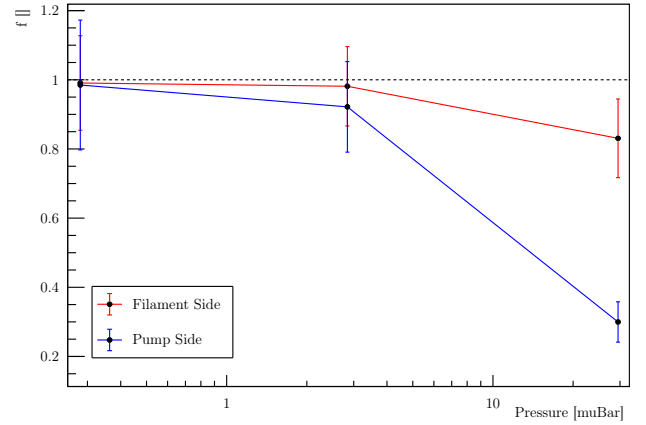
(a) Dependence on discharge polarization voltage, for a pressure of $2.84\mu\text{bar}$ and a filament current of 6.5A



(b) Dependence on discharge current, for a pressure of $2.84\mu\text{bar}$ and a filament current of 6.5A .



(c) Dependence on filament current, for a pressure of $2.84\mu\text{bar}$ and a polarization voltage of 40V .



(d) Dependence on the chamber pressure, for a filament current of 6.5A and a polarization voltage of 40V .

Figure 21: Dependence of ionization fraction on different parameters.

7 IonicSonic speed

Through the Langmuir probes, some measurements of the ionic-sonic waves propagation can be done. Igniting the plasma with a filament current of 6.5A , the grid has been polarized with a sinusoidal waves (frequency $\sim 20.8\text{kHz}$, $V_{\text{peak-peak}} \sim 50\text{V}$, which also triggers the oscilloscope) and the Langmuir probe has been connected to an oscilloscope. One of the first things noticed is that the plasma distorts the sinusoidal wave: as can be seen from fig. 22, in the output wave the rising time is greater than the falling time.

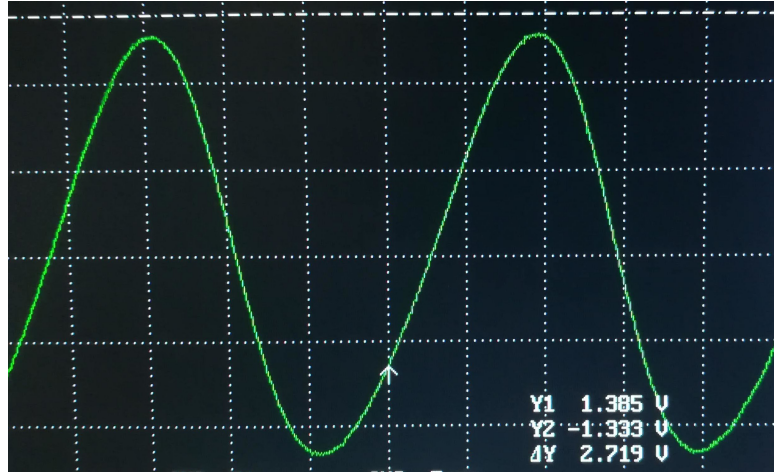


Figure 22: Signal from Langmuir probe: note the distorted sinusoidal wave. Scale: 1 square = $10\mu\text{s} \times 500\text{mV}$

Moving the probe perpendicularly to the grid, the shift of the maximum and minimum of the detected wave has been measured, and thus the speed estimated.

After various tests, searching for a configuration in which the non linear effects (i.e. the distortion of the sinusoidal wave at various position of the probe) can be neglected, the pressure has been set to around $3.26 \cdot 10^{-3}\text{mbar}$ and the polarization voltage to 36.0V . The following measurements have been done:

$\Delta x[\text{mm}]$	$\Delta t_{\min}[\mu\text{s}]$	$\Delta t_{\max}[\mu\text{s}]$
5.0 ± 0.1	2.0 ± 0.2	5.0 ± 0.2
10.0 ± 0.1	5.0 ± 0.2	7.0 ± 0.2

Table 3: IonicSonic speed: maximum and minimum shifts

By computing the speed c_s as $\Delta x/\Delta t$ in both cases and then taking the average one obtains:

$$\begin{aligned}
 c_{s,\max} &\sim 2.3 \cdot 10^3 \text{m s}^{-1} \\
 c_{s,\min} &\sim 1.3 \cdot 10^3 \text{m s}^{-1} \\
 c_s &\sim 1.8 \cdot 10^3 \text{m s}^{-1}
 \end{aligned}$$

In a first approximation,

$$c_s = \sqrt{\frac{k_B T_e}{m_i}}$$

where m_i is the Argon-ion mass ($m_i \sim 6.63 \cdot 10^{-26}\text{kg}$), which lead to an estimated electron temperature of:

$$T_e \sim 1.3\text{eV}$$

Observe that these estimations are very coarse; the used method, the available apparatus and the non-linearity terms doesn't allow a better result.

Compare with predicted one -> Guardate se va bene. Da che parte era la probe nella raccolta dei dati sperimentali di questa sezione?

When this result are compared to the experimental ones we can see that the experimental ionic-sonic speed has values near the theoretical lower bound, while experimental temperature exhibits values smaller than theoretical ones.

Nevertheless if we consider graph 17(d) and 18(d) we can see how variation of the pressure and position in the chamber raise to evident shift in electronic temperature and ionic-sonic speed. Variation of the pressure from $2.84\mu\text{bar}$ to $3.26\mu\text{bar}$ may raise to this gap between theoretical and experimental results.

8 IonicSonic decay

Keeping the same system conditions, the amplitude of the wave as function of the probe position has been studied. Moving the probe perpendicularly to the grid and recording the amplitude of the wave, the trend in fig. 23 are found.

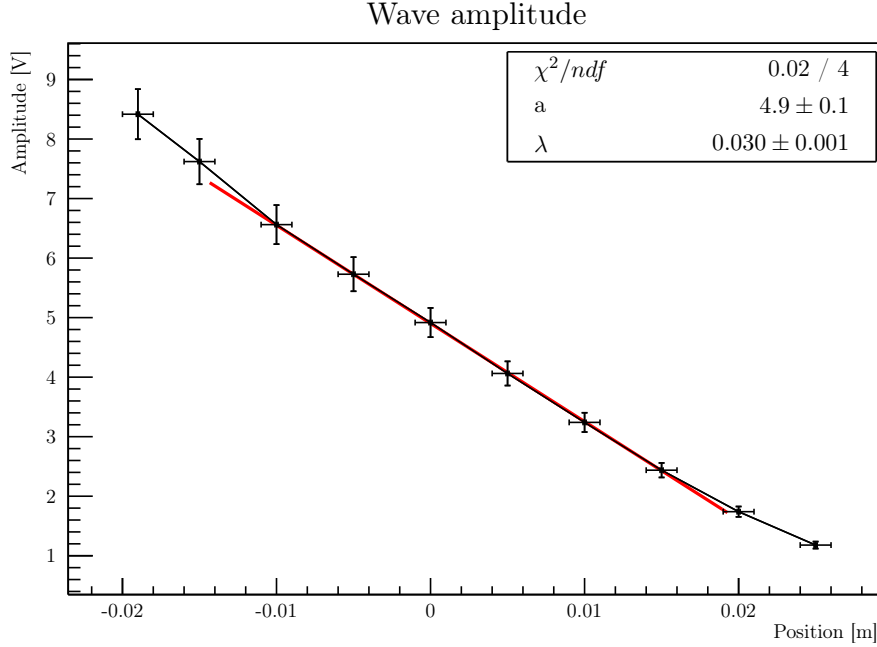


Figure 23: Peak-peak amplitude of the wave as function of the position. The 0 in the x axis has been chosen to be about around the middle of the plot.

From the theory, the amplitude should decay as an exponential. The low range explored doesn't permit a proper exponential fit, thus a first-order approximation around an arbitrary d_0 (a zero in the position is not available, therefore an arbitrary offset must be taken in account) has been done:

$$Ae^{-d/\lambda} = Ae^{-(d-d_0+d_0)/\lambda} = \underbrace{Ae^{-d_0/\lambda}}_a \left(1 - \frac{d-d_0}{\lambda}\right)$$

Having chosen in the plot the x axis such that it has the 0 around the middle of the fit range, can be assumed $x = d - d_0$. From the fit, the typical length is found:

$$\lambda = (0.030 \pm 0.001)\text{m}$$

This length can be approximated by:

$$\lambda = \frac{2c_s}{v_{te}n_0\sigma_0}$$

being σ_0 the cross section of the collisions of electrons with the neutrals ($\sigma_0 \sim 2 \cdot 10^{-20}\text{m}^2$), c_s the previous found ionic-sonic speed and v_{te} the electrons thermal speed ($v_{te} \sim \sqrt{3k_bT_e/m_e} \sim 8.4 \cdot 10^5\text{m s}^{-1}$). This lead to an estimation of the neutral particle density n_0 of:

$$n_0 \sim 7 \cdot 10^{18}\text{m}^{-3}$$

On the other hand, from the perfect-gas law, we can instead compute (assuming a temperature near to the room one, $\sim 300\text{K}$):

$$p = nk_B T \quad \rightarrow \quad n = \frac{p}{k_B T} \sim 8 \cdot 10^{19}\text{m}^{-3}$$

The two estimations are clearly incompatible: they differ from an order of magnitude. This can be due to the multiple approximations made to compute n_0 . First of all the fit: the explored range is too narrow to appreciate the exponential shape, and the trick used makes our estimation rougher. Moreover, the multiple approximate values used contribute to an inaccurate estimation of the neutral density.

9 Conclusions

With respect to the initial aims:

- By studying the vacuum, the average inflow in the chamber and the pumping speed of the pumping system have been estimated.
- By studying the V-I characteristics of the tungsten filament the relation between the filament current and its temperature has been found.
- The V-I characteristics of the plasma in DC condition has been found and the Paschen curve built: both of them show relevant deviation from the theory.
- Paschen RF results
- Langmuir probes results
- By inducing a sonic wave in the plasma the ionic sonic speed and the wave exponential damping have been estimated.

Commenti sulla dipendenza di V_f da V .

Dire qualcosa sul fatto che le due stime di n_0 differiscono di un'ordine di grandezza